Composite Structures 182 (2017) 1–11

Contents lists available at ScienceDirect

Composite Structures

journal homepage: www.elsevier.com/locate/compstruct

Small perforations in corrugated sandwich panel significantly enhance low frequency sound absorption and transmission loss

H. Meng [a,b,c], M.A. Galland [b,*], M. Ichchou [c,*], O. Bareille [c], F.X. Xin [a,d], T.J. Lu [a,d]

[a] MOE Key Laboratory for Multifunctional Materials and Structures, Xi'an Jiaotong University, Xi'an 710049, PR China
[b] Univ Lyon, École Centrale de Lyon, Laboratoire de Mécanique des Fluides et d'Acoustique, UMR CNRS 5509, F-69134 Écully, France
[c] Laboratoire de Tribologie et Dynamique des Systèmes, École Centrale deLyon, 36, Avenue Guy de Collongues, 69130 Ecully Cedex, France
[d] State Key Laboratory for Strength and Vibration of Mechanical Structures, Xi'an Jiaotong University, Xi'an 710049, PR China

ARTICLE INFO

Article history:
Received 29 May 2017
Revised 27 August 2017
Accepted 29 August 2017
Available online 6 September 2017

Keywords:
Corrugated sandwich panel
SAC
STL
Perforation
Multifunctional application

ABSTRACT

Numerical and experimental investigations are performed to evaluate the low frequency sound absorption coefficient (SAC) and sound transmission loss (STL) of corrugated sandwich panels with different perforation configurations, including perforations in one of the face plates, in the corrugated core, and in both the face plate and the corrugated core. Finite element (FE) models are constructed with considerations of acoustic-structure interactions and viscous and thermal energy dissipations inside the perforations. The validity of FE calculations is checked against experimental measurements with the tested samples provided by additive manufacturing. Compared with the classical corrugated sandwich without perforation, the corrugated sandwich with perforated pores in one of its face plate not only exhibits a higher SAC at low frequencies but also a better STL as a consequence of the enlarged SAC. The influences of perforation diameter and perforation ratio on the vibroacoustic performance of the sandwich are also explored. For a corrugated sandwich with uniform perforations, the acoustical resonance frequencies and bandwidth in its SAC and STL curves decrease with increasing pore diameter and decreasing perforation ratio. Non-uniform perforation diameters and perforation ratios result in larger bandwidth and lower acoustical resonance frequencies relative to the case of uniform perforations. The proposed perforated sandwich panels with corrugated cores are attractive ultralightweight structures for multifunctional applications such as simultaneous load-bearing, energy absorption, sound proofing and sound absorption.

1. Introduction

Sound transmission loss (STL) and sound absorption coefficient (SAC) of panels are the two biggest acoustic issues for investigators in this area in the past decades. The most appealing structures for sound transmission are sandwich structures made of multiple-layer panels and cores [1–8]. Sandwich panels can be designed to have low density, high stiffness-to-mass ratio, and excellent thermal and acoustic characteristics, and hence have been widely applied as soundproof concepts. Many kinds of cores exist for sandwich construction, such as air cavity, foams, honeycombs and corrugations (folded plates), to mention just a few. Extensive investigations have been devoted to evaluating the STL of a wide range of sandwich panels, which may be classified by the core types.

Double wall partitions with air cavity, perhaps the simplest sandwich construction, received much attention [9–15]. For example, Wang et al. [9] calculated the STL of double leafs with enclosed air cavity numerically using the statistical energy analysis approach, while Xin et al. [10] analytically predicted the STL of simply supported finite double leaf panels with air cavity. Instead of air cavity, numerous studies have also been carried out on sandwich panels with sound absorbing cores [6,7,16–23]. For instance, Bolton et al. [18,21] presented calculations of STL of double-panel structures lined with elastic porous material by applying the Biot theory, and Doutres and Atalla [17] proposed a theory to estimate the STL of double panel structures with multilayered absorbing blanket cores. Sandwich panels with sound absorbing cores turned out to improve the STL at structural resonance frequencies. With excellent mechanical efficiency, sandwich panels with honeycomb cores are more widely used in applications than those with air or

* Corresponding authors.
E-mail addresses: marie-annick.galland@ec-lyon.fr (M.A. Galland), mohamed.ichchou@ec-lyon.fr (M. Ichchou).

http://dx.doi.org/10.1016/j.compstruct.2017.08.103
0263-8223/

sound absorbing cores. It is therefore natural that the STL of honeycomb sandwich panels has been extensively investigated [8,24–30]. Jung et al. [27] presented a theory to predict the STL of honeycomb sandwich by assuming the core is homogeneous orthotropic. Griese et al. [28] numerically calculated the STL performance of honeycomb sandwiches and analyzed the effect of core geometry. Zhou and Crocker [25] presented STL calculations of foam-filled honeycomb sandwich panels by statistical energy analysis. Rajaram et al. [29] investigated the effects of panel design parameters on the STL of honeycomb sandwiches. Tang et al. [26] presented a model to estimate the STL of cylindrical sandwich shell with honeycomb core. Among all the sandwich constructions, sandwich panels with corrugated cores are perhaps the most appealing alternative in the transportation industry (e.g., high speed train) due to excellent mechanical performance with limited thickness, simple two-dimensional (2D) configuration, structural stability and easy manufacture procedure. Shen et al. [31] and Xin et al. [32] presented analytical STL investigations of corrugated sandwich panels by modelling the corrugated core as translational and rotational springs. Bartolozzi et al. [33] calculated the sound transmission loss of sandwich panels with sinusoidal corrugated cores by treating the corrugated cores as an equivalent homogenous material. Nonetheless, despite the success applications of sandwich panels for settling the issue of STL, they are incapable of sound absorption.

On the contrary, micro-perforated panels (MPPs) are effective sound absorbers. MPPs are usually comprised of plates with submillimeter pores, an air cavity, and a rigid wall. The sound absorption mechanism of the MPPs is closely connected to the classical Helmholtz resonance absorption. Compared with the traditional sound absorbing materials, MPPs are more environment-friendly and suitable for severe situations, such as high temperature, high pressure, or presence of water. The sound absorption performance of the MPPs has been investigated, both theoretically and experimentally, by many investigators. Applying the method of electroacoustic analogy, Maa [34,35] first proposed an analysis model for the SAC of single and double MPPs. While Atalla and Sgard [36] attempted to evaluate the SAC of MPPs by employing rigid frame porous material models, Rao and Munjal [37] and Lee and Kwon [38] used an empirical impedance model to estimate the SAC of MPPs. Although efficient in SAC, MPPs are invalid structures for STL. Studies by Chen [39] and Dupont et al. [40] demonstrated that the STL of a MPP is even smaller than that of a single plate having the same thickness.

Nowadays, combinations of MPP and sandwich structures come into the view of researchers concerning both the STL and SAC of panels. Perforated pores in the face plates of the sandwich panels can provide effective sound absorption as MPP layers, while the backed plates and core structures can act as sound insulation barriers. Dupont et al. [40] first investigated the acoustic properties of a MPP coupling with a flexible plate both analytically and experimentally. It was found that the coupled MPP-air cavity-plate system could increase the STL while maintaining a good SAC. To improve the STL at mid frequencies, Toyoda and Takahashi [41] subdivided the air cavity of the MPP-air cavity-plate system by inserting honeycomb structures to the air cavity. Bravo et al. [42,43] proposed a fully coupled modeling approach to calculate the SAC and STL of single or multi-layer MPPs and plates. It was shown that the SAC and STL at acoustical resonance frequencies were controlled by the relative velocities of air-frame and the MPP-back panel. Mu et al. [44] added MPP layer both to the source and the transmitted side of double leaf panels and found that the MPP layer weakened the mass-air-mass resonance.

The investigations as discussed above concern the acoustical properties of sandwich panels with face plate perforations. The middle cores of these sandwich panels are air gap or honeycomb structures. None of these investigations considers corrugated sandwich panels with perforations. In addition to load-bearing, corrugated sandwich panels are an appealing structure for STL in application. Different from the honeycomb sandwich panels, corrugated sandwich panels can have perforations in the corrugated pores as well as in the face plates (see Fig. 1). It will be interesting for investigators in this area to see how the SAC and STL are affected by various perforation configurations in corrugated sandwich panels.

Perforations in the corrugated sandwich panels are often microsized that makes the manufacture of perforated sandwich panels extremely difficult by conventional manufacturing methods. Hence, the additive manufacturing (also known as 3D printing) is employed to fabricate the perforated corrugated sandwiches. In an additive manufacturing progress, the expected structure is created by laying down thin layers of materials according to the dig-

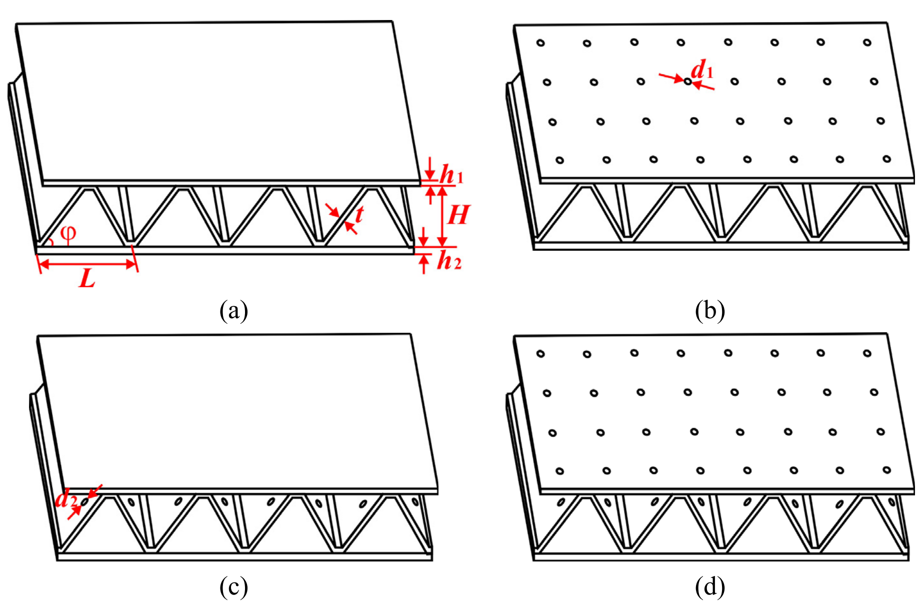

Fig. 1. Schematic of classical corrugated sandwich panel and corrugated sandwich panels with various perforation configurations.

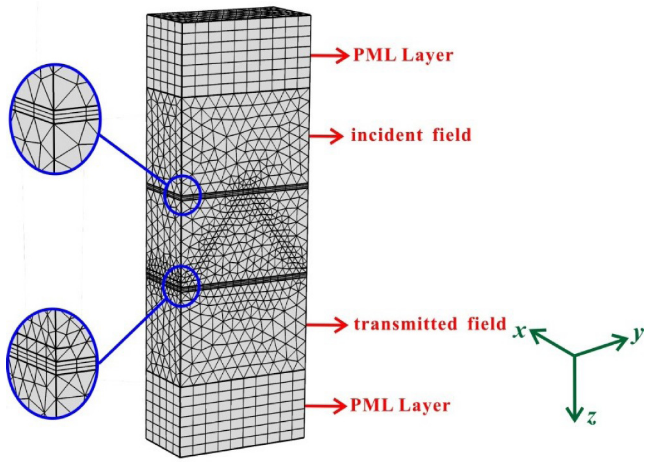

Fig. 2. Finite element model of a unit cell of corrugated sandwich panel.

ital CAD models. Nowadays, there exist many different kinds of 3D printers, including direct metal laser sintering (DMLS), selective laser melting (SLM), fused deposition modeling (FDM), etc. [45]. These 3D printers can create objects from many materials, plastics, sandstones, porcelains, pure metals, alloys and almost everything in-between. The additive manufacturing can not only print structures with elaborate shapes, it is also a more time-saving method than conventional manufacturing methods for single or small batch production [46–49].

This study deals with the SAC and STL of corrugated sandwich panels with perforations at normal incidence of sound. Section 2 presents the FE (finite element) models to calculate the SAC and STL of corrugated sandwich panels with different perforation configurations. Section 3 describes an experiment conducted in an impedance tube for the validation of the FE models. Based on the FE models proposed in Section 2, Section 4 compares the SAC and STL of corrugated sandwich panels with different perforation configurations. The influences of the perforated pore diameter and porosity are also discussed in Section 4.

2. Corrugated sandwich panels with perforations: FE simulation

Fig. 1 presents 4 kinds of corrugated sandwich panels with different perforation configurations. The sample in Fig. 1(a) represents classical corrugated sandwich panels without perforation. The wall thicknesses of the two face plates and the corrugated core are h_1, h_2 and t, respectively. The distance between the two face plates is H. The inclination angle of the corrugated core is φ, and the width of the unit cell of the corrugated core is L. Samples in Fig. 1(b)–(d) have perforated pores of submillimeter$\sim$millimeter scale in the upper face plate, in the corrugated core, and in both the upper face and the core, respectively. The diameters of perforated pores in the face plate and the corrugated core are d_1 and d_2 respectively. It is noted that for all these corrugated sandwich panels, no perforated pores exist on the lower face plate to achieve more effective STL.

When a plane wave impinges on the upper face plate, the acoustical properties of the corrugated sandwich panel can be calculated by the FE model shown in Fig. 2. The FE model is set up by using COMSOL Multiphysics. The plane wave is applied to the incidence field. The Perfectly Match layer (PML) is a domain that can absorb all the energy entering into it, and waves impinge on the PML from other non-PML domains won't be reflected. Therefore, two Perfectly Match layers (PML) are added to the ends of incident and the transmitted fields to simulate infinite and non-reflecting acoustic domain.

The air in the incident, transmitted and middle fields is compressible but lossless flow, with no thermal conductivity and viscosity considered. Thus the 'Pressure Acoustics' module of COMSOL, which is suited for all frequency-domain simulations with harmonic variations of the pressure field, is applied. The sound pressure is governed by the Helmholtz equation in this module:

$$\nabla^2 P = \frac{1}{c_0^2}\frac{\partial^2 P}{\partial t^2} \tag{1}$$

where P is the sound pressure of the pressure acoustic field, t is the time and c_0 is the sound speed.

The solid components of the structures are taken as isotropic linear elastic materials, with the 'Solid Mechanics' module of COMOL applied during the simulation. The displacement of the panel is governed by:

$$-\rho\omega^2\mathbf{u} - \frac{1}{2}\nabla\cdot\mathbf{C} : ((\nabla\mathbf{u})^{\mathrm{T}} + \nabla\mathbf{u}) = 0 \tag{2}$$

where $\mathbf{u}$ represents the displacement of the solid panel, ρ is the density of the solid panel, ω is the angular frequency, : represents double contraction, $\mathbf{C}$ is the elastic tensor of the panel material, which actually can be expressed by two elastic constants (i.e., the Young's modulus and the Poisson ratio) for isotropic elastic material.

As to the air inside the small pores, the radius of the pores is of comparable size with the thermal boundary thickness and viscous boundary thickness at low frequencies, which means the thermal conduction and viscosity should be considered during the simulation. Therefore, the 'Thermal-Acoustics' module is applied. The sound pressure, temperature, and particle velocity are governed by three equations, namely, the linear Navier-Stokes equation, the mass continuity equation, and the heat conduction equation in this module:

$$\begin{aligned} & i\omega\rho_0\mathbf{v} = \nabla\cdot(-P_t\mathbf{I} + \eta(\nabla\mathbf{v} + (\nabla\mathbf{v})^{\mathrm{T}}) - \tfrac{2}{3}\eta(\nabla\cdot\mathbf{v})\mathbf{I}) \\ & i\omega\rho_0(\tfrac{P_t}{P_0} - \tfrac{T}{T_0}) + \rho_0\nabla\cdot\mathbf{v} = 0 \\ & i\omega\rho_0 C_p T = -\nabla\cdot(-K_T\nabla T) + i\omega P_t \end{aligned} \tag{3}$$

where $\mathbf{v}$ is the fluid velocity, and T is the temperature variation, P_t is the sound pressure of the thermal-acoustic field, ρ_0 is the density of air, η is the dynamic viscosity, C_p denotes the heat capacity of air at constant pressure, and K_T is the thermal conductivity, $\mathbf{I}$ is the identity matrix. Besides, P_0 and T_0 represent equilibrium pressure and temperature.

At the interface of the pressure acoustic field and solid panel, the normal accelerations of the air and panel are the same in the FE model, given as

$$-\mathbf{n}\cdot\left(\tfrac{-1}{\rho_0}\nabla P\right) = -\mathbf{n}\cdot\mathbf{a}_t \quad \mathbf{F}_A = P\mathbf{n} \tag{4}$$

where $\mathbf{n}$ is the surface normal direction, $\mathbf{a}_t$ is the acceleration of the solid panel. $\mathbf{F}_A$ is the total load of solid panel, which is decided by the normal sound pressure exerted on the panel.

While at the interface of the thermal acoustic field and pressure acoustic field, the continuous normal stress and acceleration and adiabatic conditions are applied in the FE model, as

$$\begin{aligned} & \left(-P_t\mathbf{I} + \eta(\nabla\mathbf{v} + (\nabla\mathbf{v})^{\mathrm{T}}) - \tfrac{2}{3}\eta(\nabla\cdot\mathbf{v})\mathbf{I}\right)\mathbf{n} = -P\mathbf{n} \\ & -\mathbf{n}\cdot\left(\tfrac{-1}{\rho_0}\nabla P\right) = -\mathbf{n}\cdot i\omega\mathbf{v} \\ & -\mathbf{n}\cdot(-K_T\nabla T) = 0 \end{aligned} \tag{5}$$

As to the thermal acoustic field and solid panel coupling boundary, the velocity of the air is identical to that of the solid panel and the temperature variation is isothermal at the interface of the two fields in the FE model,

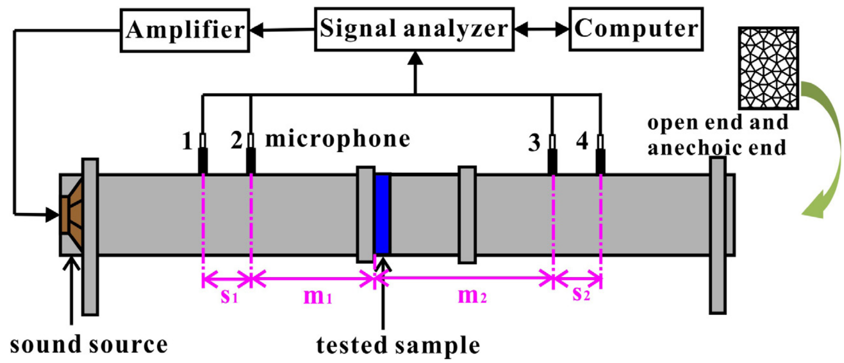

(a)

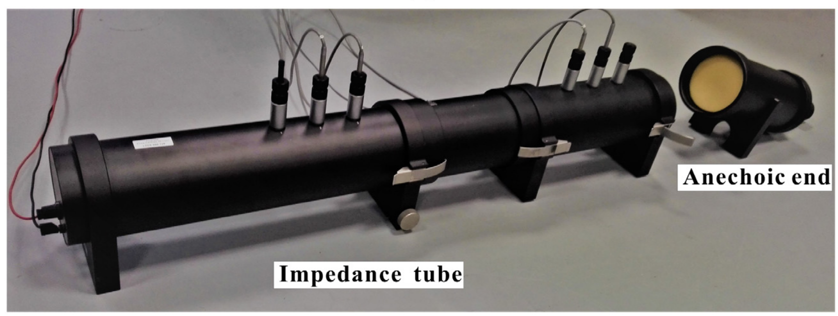

(b)

Fig. 3. (a) Schematic of the experimental system, (b) Photograph of the impedance tube.

$$\begin{aligned} \mathbf{v} &= i\omega\mathbf{u} \\ T &= 0 \end{aligned} \tag{6}$$

For corrugated sandwich panels of infinite size, FE simulations can be conducted using a unit cell with periodic boundary conditions as shown in Fig. 2. In contrast, for panels of finite size, the whole panel with actual boundaries should be embodied in the FE model. Model settings for the air and solid frame previously mentioned are applicable for both infinite and finite sized samples. Most part of the FE model is meshed by tetrahedral elements except from the plates and PML as shown in Fig. 2. The PMLs use the swept mesh method to create triangular prism elements as suggested in the User's Guide Manual of Comsol. The plates are also meshed by the swept mesh method due to the high transverse length to thickness ratio. Elements sizes changes with the dimension of each part.

The energy of sound is divided into three parts during its propagation through the composite panel, as:

$$E = E_{ref} + E_{trans} + E_{absorp} \tag{7}$$

where E_{ref} denotes the reflected energy in the incident field, E_{trans} denotes the transmitted energy in the transmitted sound field, while E_{absorp} denotes the absorbed energy inside the sandwich panel. In the FE model, a normal incidence sound wave with pressure $P_{xi} = e^{-ik_0 z}$ is incident on the surface of the panel, thus the total sound energy is:

$$E = \frac{1}{2}\mathrm{Re}\int_S P_i \cdot v_i^* dS \tag{8}$$

where $k_0 = \frac{\omega}{c_0}$, S is the area of incidence plane of the FE model. v_i is the velocity of incident wave, given as $v_i = \frac{-1}{i\omega\rho_0}\frac{\partial P_i}{\partial z} = \frac{e^{-ik_0 z}}{\rho_0 c_0}$

The reflected sound energy E_{ref} is calculated by:

$$E_{ref} = \frac{1}{2}\mathrm{Re}\int_S \{(P_1 - P_i)\cdot(-v_1 + v_i)^*\}dS \tag{9}$$

where P_1 and v_1 are the total sound pressure and velocity at the surface of the top face plate in the incident field. $(P_1 - P_i)$, $(-v_1 + v_i)$ represent the reflected sound pressure and velocity at the surface of the top face plate in the incident field respectively.

The transmitted energy E_{trans} is given as:

$$E_{trans} = \frac{1}{2}\mathrm{Re}\int_S P_3 \cdot v_3^* dS \tag{10}$$

where P_3 and v_3 are the sound pressure and velocity at the surface of the bottom face plate in the transmitted field. Hence, the STL can be obtained as:

$$TL = 10\log_{10}\frac{E}{E_{trans}} \tag{11}$$

while the SAC is written as:

$$\alpha = 1 - \frac{E_{trans}}{E} - \frac{E_{ref}}{E} \tag{12}$$

3. Experimental validation

Experimental measurements were performed to validate the FE models by using the four microphones B & K standing wave tube with the two load method shown in Fig. 3(a) and (b). A loudspeaker mounted at the end of the tube was set to generate a random noise signal over the frequency span of 100–1600 Hz. Four microphones were installed at four measuring positions to measure the frequency response functions. Notice that B&K 4206 large tubes with a diameter of 100 mm were chosen, suitable for low frequency measurement (100–1600 Hz). As shown in Fig. 3 (a), distances between microphones s_1 and s_2 are 50 mm, and distances between the tested sample and microphones m_1 and m_2 are 100 mm and 250 mm respectively. The two-cavity method developed by Bolton et al. [50] was applied to obtain the acoustic properties of the

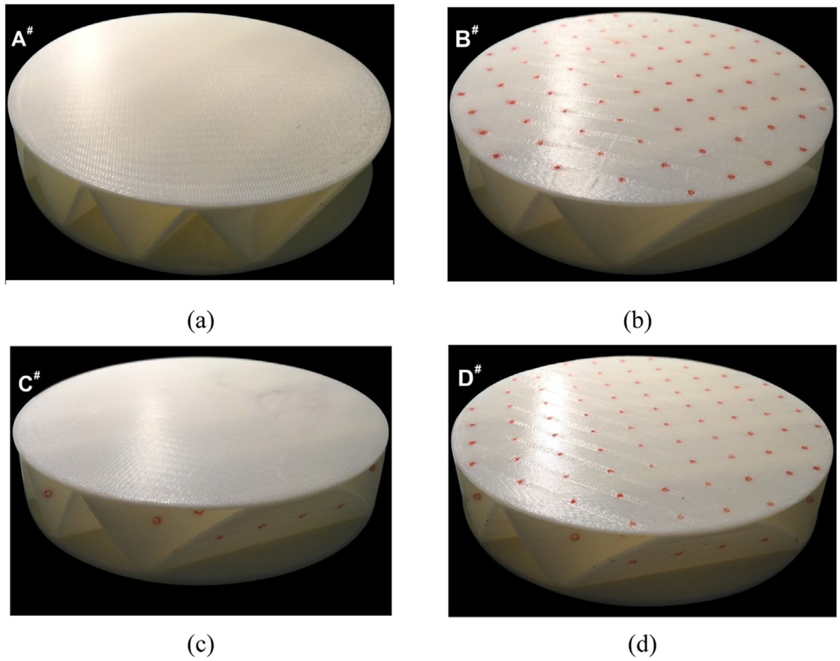

Fig. 4. Pictures of corrugated sandwich panel samples for impedance tube test, (a) Samples A#, (b) Sample B#, (c) Sample C#, (d) Sample D#.

Table 1
Geometrical parameters of corrugated sandwich samples for experiment.

Parameters	Value
face plate thicknesses	$h_1 = 1$ mm $h_2 = 2$ mm
distance between face plates	$H = 17$ mm
perforation ratios	$\sigma_1 = \sigma_2 = 0.78\%$
pores diameters	$d_1 = d_2 = 1$ mm
thickness of core plate	$t = 1$ mm
inclination angle of core plate	$\varphi = 63.4^\circ$
unit cell width of core	$L = 20$ mm

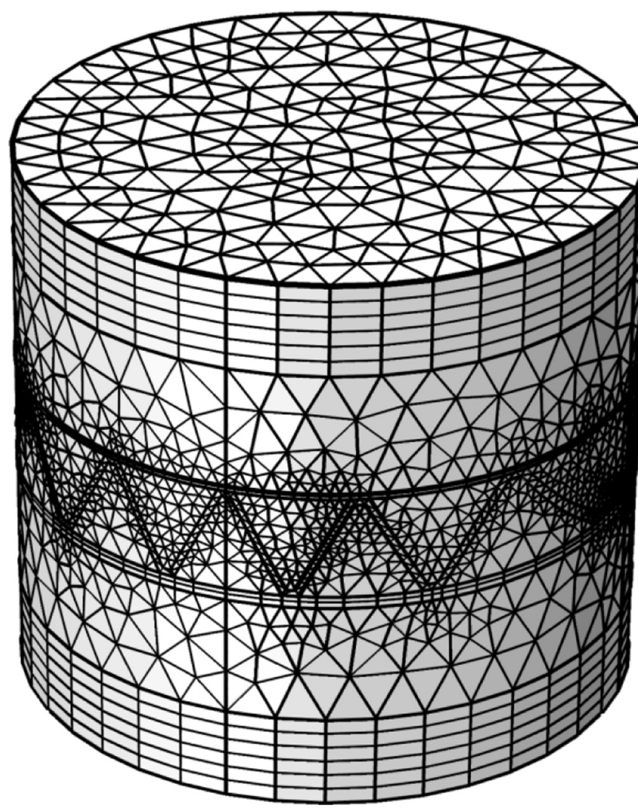

Fig. 5. Representative FE model for test sample.

tested samples. The transfer matrix elements were solved by two independent measurements, conducted separately with open tube termination and anechoic termination. The fully absorbing termination was created with 3 standard sound absorbing samples having an approximately 75 mm depth in total.

Fig. 4 shows the four test samples A#, B#, C# and D#, corresponding to the four types of panel in Fig. 1. The samples were manufactured using a FDM 3D printer with a density of 958 kg/m^3, Young's modulus of 1 GPa and Poisson' ratio of 0.35. Geometrical parameters of the samples are listed in Table 1. The perforation ratio in Table 1 is defined as the ratio of the area of the perforated pores to the area of the sandwich panels. During the measurement, the samples were fixed in the tube. FE models of finite size identical to the tested samples are set up (see Fig. 5) by applying the FE method presented in the previous section. Fixed constrains and sound hard wall boundary conditions are applied to the boundaries of the solid panel and pressure acoustic field of the FE models respectively. The meshes of the calculated FE models are shown in Fig. 5 with the convergences checked by mesh refinement. Physical parameters of the air are shown in Table 2.

Fig. 6 compares the measured STLs with those obtained from FE simulations. The experimental data agree well with the simulation results for all four samples, demonstrating that the FE method presented is effective to estimate the acoustical properties of corrugated sandwich panels with or without perforations. It is noted that different from the infinite sized samples, the stiffness of finite sized tested samples is enhanced by the fixed boundary conditions, thus the sound transmission loss decreases with frequency within the stiffness controlled frequency region until the first structural resonance frequency. The first structural resonance frequencies for these samples exist around 2000 Hz which exceeds the tested frequency range, so the sound transmission loss drops with fre-

Table 2
Physical parameters of air.

Parameters	Value
density	$\rho_0 = 1.21\ \text{kg/m}^3$
sound speed	$c_0 = 343\ \text{m/s}$
the equilibrium pressure	$P_0 = 101320\ \text{Pa}$
temperature	$T_0 = 293.15\ \text{K}$
dynamic viscosity	$\eta = 1.81 \times 10^{-5}\ \text{Pa} \cdot \text{s}$
thermal conductivity	$K_T = 0.026\ \text{W}/(\text{m} \cdot \text{K})$
heat capacity at constant pressure	$C_p = 1004\ \text{J}/(\text{kg} \cdot \text{K})$

quency as shown in Fig. 6. The deviations between simulation and experimental STLs at low frequencies are mainly introduced by the non-ideal experimental conditions, including air leaks at the interface between sample edges and impedance tube, measuring errors by microphones, etc.

The comparisons between the SACs by FE simulations and experiments are shown in Fig. 7(a)–(d). It can be seen from Fig. 7 that the FE simulations can give reasonable estimations for the SACs. For Samples A# and C#, both the SACs by FE simulation and experiments are close to zero. For Samples B and D, the SACs by FE simulations capture the resonances frequencies precisely, however, the bandwidths of measured SACs are bigger than simulation results. The discrepancies of the bandwidth are mainly caused by the inevitable manufacturing errors, such as the irregular edge shapes of the perforated pores and extra mini pores adjacent to perforated pores. Besides, the peak values in the experimental SAC curves are smaller than that in the numerical SAC curves, which may be attributed to the non-ideal experimental conditions. In addition, discrepancies are also introduced by assumptions of the FE models. For instance, density fluctuation of the air by the temperature variation is ignored in FE models, fixed boundary conditions are ideally assumed without any air leaks during simulation process.

4. Results and discussion

4.1. Influence of perforation configurations

Based on the FE models proposed and validated in previous sections, the STL and SAC of the four kinds of corrugated sandwich panels are compared next. For simplification, sandwich panels of infinite size are considered. These panels are assumed to be made of aluminum with a density of 2700 kg/m^3, Young's modulus of 70 GPa, and Poisson's ratio of 0.33.

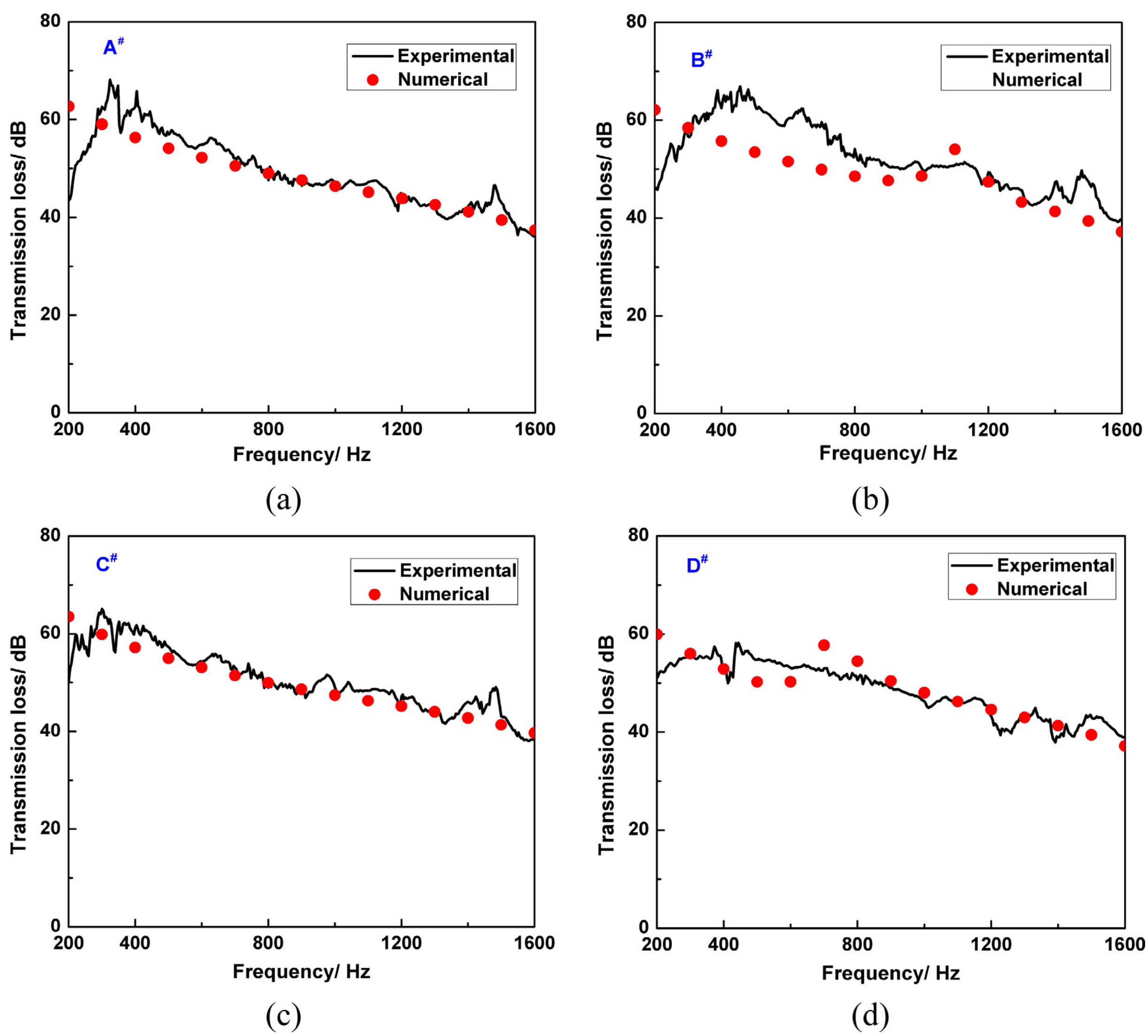

Fig. 6. Comparison between the STLs obtained by FE simulation and experimental measurement, (a) Samples A#, (b) Sample B#, (c) Sample C#, (d) Sample D#.

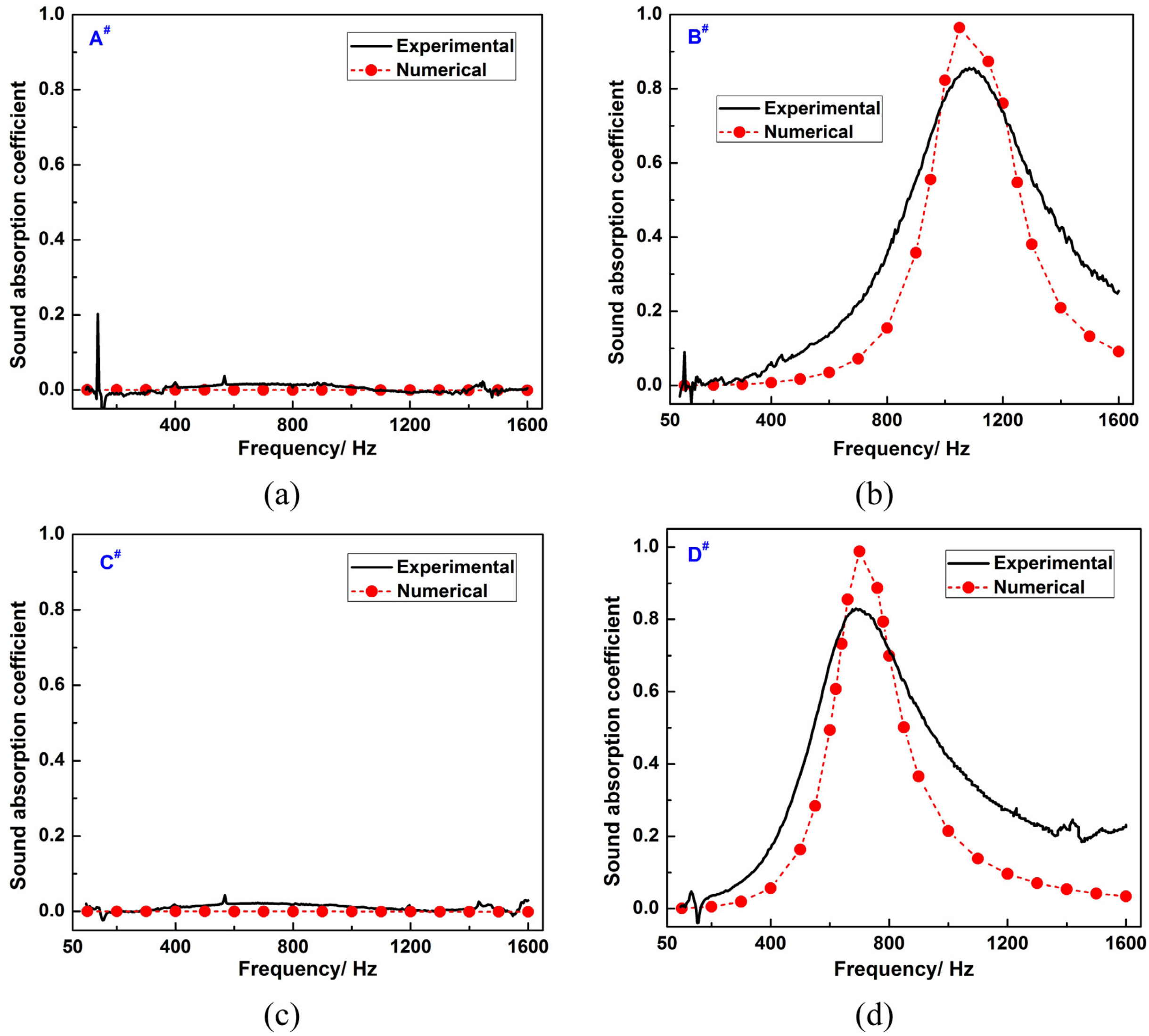

Fig. 7. Comparison between the SACs obtained by FE simulation and experimental measurement, (a) Samples A#, (b) Sample B#, (c) Sample C#, (d) Sample D#.

The STL and SAC of the classical corrugated sandwich panel are compared with those of corrugated sandwich panels with various perforation configurations in Figs. 8 and 9, with the geometrical parameters of these panels listed in Table 3. It can be seen that, compared with classical panels, panels with perforations in the face plate have better SAC and STL at low frequencies, while those with perforations only in the corrugated core have almost identical STL and SAC curves. For panels with face plate perforations, the sound waves can enter the small pores during propagation. As a result, the SAC can be dramatically enlarged since the sound energy is consumed by viscous and thermal dissipations inside the pores. Due to the improvement of absorbed energy, the transmitted energy is reduced and hence the STL is enlarged. On the contrary, for a panel with perforations only in the core, most of the sound is reflected by the upper face plate. Correspondingly, the SAC is negligibly small and no improvement occurs in the STL. Besides, it also can be seen that acoustical resonance frequencies exist in the SAC and STL curves of panels with face plate perforations. Panel with perforations in both the face plate and the core have lower acoustical resonance frequency than that of panel with only face plate perforations.

It can be concluded that perforations have great influence on the STL and SAC of corrugated sandwich panels, with those having

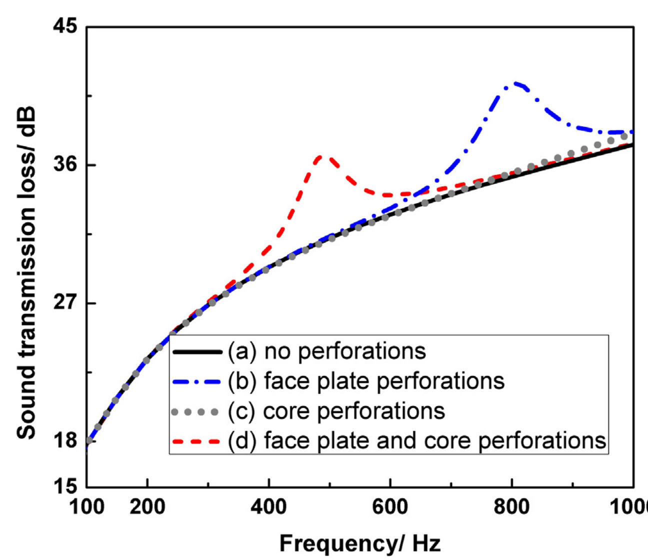

Fig. 8. STL comparison among corrugated sandwich panels with different perforation configurations.

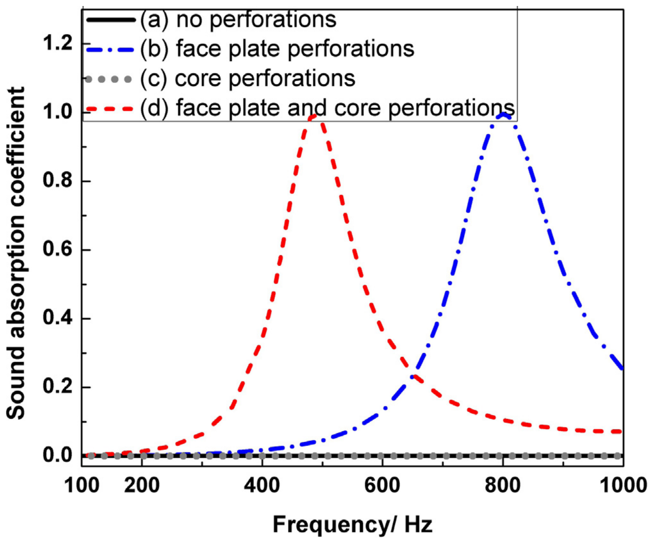

Fig. 9. SAC comparison among corrugated sandwich panels with different perforation configurations.

perforations both in the face plate and the core exhibiting the best acoustic performance at low frequencies. Hence, further study of the perforations is conducted based on panels with both face plate and core perforations. The effects of pore diameter and pore size are discussed in the following section.

4.2. Influence of pore diameter

Fig. 10 compares the STL and SAC of three corrugated sandwich panels having identical geometrical parameters (as listed in Table 3) apart from the perforated pore diameters. For all the three sandwich panels, the pore diameters are uniformly distributed, namely, the diameter of pores in the face plate is equal to that in the corrugated core. It can be seen from Fig. 10 that, with decreasing pore diameter, the bandwidth of SAC increases. When the perforation ratio is fixed, the air-frame interfacial area inside the perforated pores increases as the pore diameter is reduced. The improved air-frame interface area increases the acoustic resistance, enlarging the bandwidth in SAC and STL as a consequence. It also can be seen from Fig. 10 that decrease in pore diameter can enlarge the acoustical resonance frequencies and reduce the peak values in STL and SAC curves. As is known, the acoustical resonance frequency of micro perforated structures is dominated by their acoustic reactance. Since decreasing pore diameter can reduce the acoustic reactance, hence enlarges the acoustical resonance frequency [51,52].

Table 3
Geometrical parameters of the calculated corrugated sandwich panels.

Parameters	Value
face plates thicknesses	$h_1 = h_2 = 1$ mm
distance between face plates	$H = 18$ mm
perforation ratios	$\sigma_1 = \sigma_2 = 0.349\%$
pores diameters	$d_1 = d_2 = 1$ mm
thickness of core plate	$t = 1$ mm
inclination angle of the core	$\varphi = 54.8^\circ$
unit cell width of the core	$L = 30$ mm

Corrugated sandwich panels are ideally expected to have high peak values, big bandwidths and low acoustical resonance frequencies in SAC and STL curves at the same time. However, for sandwich panels with uniform pore diameters, the results of Fig. 10 reveal that there exists a contradiction among increment of bandwidth, decrease of acoustical resonance frequencies and increment of peak values. Therefore, panels with non-uniform pore diameters are resorted to balance this problem as shown in Fig. 11.

Fig. 11 compares the STL and SAC of sandwich panels having both uniform and non-uniform perforations. For the two non-uniformly perforated sandwich panels, if the pores in the face plate have larger diameter than that in the corrugated cores, the pore diameters are defined as in descending order, otherwise they are defined as in ascending order. It can be seen from Fig. 11 that non-uniform pores can remedy the aforementioned deficiency induced by uniform pores. Compared with the uniformly perforated sandwich panels with pore diameter of 1 mm, the non-uniformly perforated panels have larger acoustic resistance induced by smaller pores in the face plates or corrugated cores, therefore, they exhibit wider bandwidth. On the other hand, the non-uniformly perforated panels have bigger pores in the face plates or corrugated cores than the uniformly perforated sandwich panels with pore diameter of 0.5 mm, which will enlarge the acoustic reactance of the panel, hence reduce the acoustical resonance frequency. In addition, the results of Fig. 11 also show that panels with non-uniform pores diameters in descending order have better STL and SAC at low frequencies than those in ascending

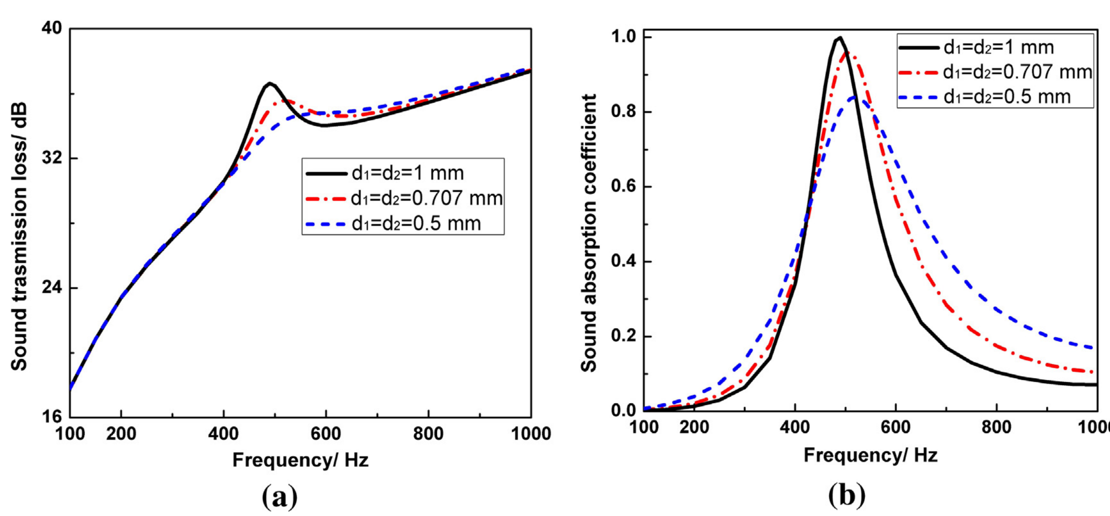

Fig. 10. STL and SAC comparison among corrugated sandwich panels with uniform perforations but different pore diameters, (a) STL comparison, (b) SAC comparison.

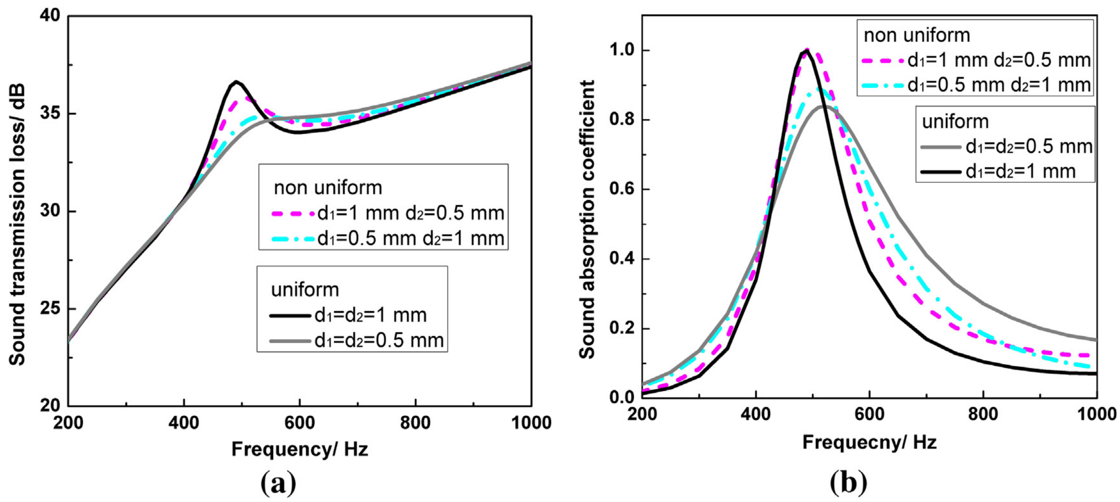

Fig. 11. STL and SAC comparison among corrugated sandwich panels with perforations of uniform pore diameters and those with non-uniform pore diameters, (a) STL comparison, (b) SAC comparison.

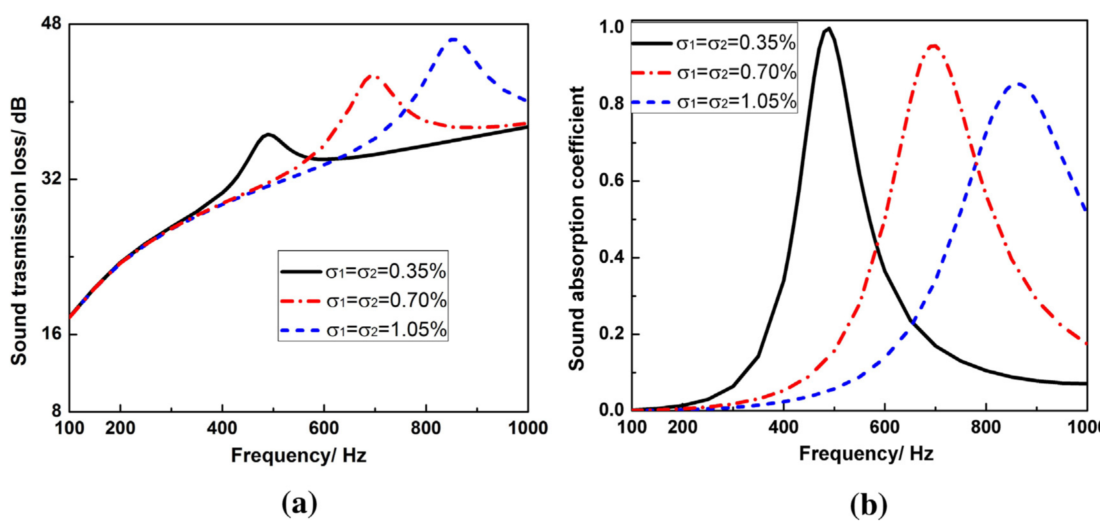

Fig. 12. STL and SAC comparison among corrugated sandwich panels with perforations of different porosities, (a) STL comparison, (b) SAC comparison.

order. For double layer coupled micro perforated structures, the coupling reaction between the two perforated layers is decided by the acoustic reactance of the layer farther from the sound source. Increase of the coupling reaction can result in bigger acoustical resonance frequency [52]. The coupling effect of the panel with pore diameters in ascending order is larger than that with pore diameters in descending order due to the bigger pore diameter and acoustic reactance of the corrugated core. Therefore, the non-uniformly perforated panel with pores diameters in ascending order generates higher acoustical resonance frequency.

4.3. Influence of perforation ratio

This subsection discusses the influence of perforation ratio on the STL and SAC of corrugated sandwich panels. These perforated panels have the same geometrical parameters (as listed in Table 3) except perforation ratios. Notice that for the three sandwich panels discussed in Fig. 12, the perforation ratio in the face plate is identical to that in the corrugated core of the same sandwich panel. It can be seen from Fig. 12 that, for both STL and SAC, the bandwidth is enlarged as the perforation ratio is increased, which can also be attributed to the increasing acoustic resistance by increasing porosity. Besides, the acoustical resonance frequency decreases with decreasing perforation ratio owing to the enlarged acoustic reactance. Contradiction between the decrease of acoustical resonance frequency and the increase of bandwidth also exists for panels with uniform perforation ratios. Therefore, panels with non-uniform perforation ratio are explored in Fig. 13.

The STL and SAC of corrugated sandwich panels with non-uniform perforation ratios are compared with those with uniform perforation ratios in Fig. 13. The perforation ratios of the face plate and that of the core are in descending order and ascending order, respectively. Attributed to the enlargement of acoustic reactance induced by the smaller perforation ratio in the face plate or corrugated core, the panel with non-uniform perforation ratio is seen to have a lower acoustical resonance frequency than the uniformly perforated panel with a perforation ratio of 1.05%. On the other hand, the panel with non-uniform perforation ratio possess bigger acoustic resistance because of the bigger perforation ratio in the

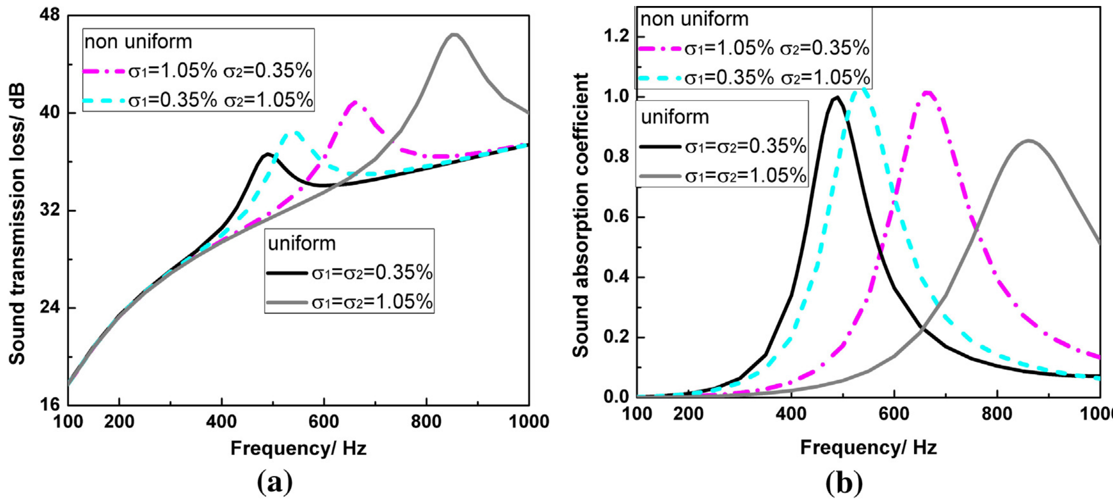

Fig. 13. STL and SAC comparison among corrugated sandwich panels with perforations of uniform and non-uniform porosities, (a) STL comparison, (b) SAC comparison.

face plate or corrugated core than the uniformly perforated panel with a perforation ratio of 0.35%, which results in broader bandwidth. Besides, it also can be seen from Fig. 13 that sandwich panels with non-uniform perforation ratios in ascending order have better STL and SAC at low frequencies than that in descending order. As mentioned in Section 4.2, the acoustical resonance frequencies of the two non-uniformly perforated panel are related to the acoustic reactance of the corrugated cores. The non-uniformly perforated panel with descending perforation ratios has corrugated core with larger acoustic reactance, therefore, exhibits higher acoustical resonance frequencies than the other panel.

5. Conclusions

In this study, corrugated sandwich panels with perforations are numerically investigated from the SAC and STL viewpoint. Finite element models are constructed by applying Comsol Multiphysics. The numerically calculated STLs are validated by comparing with experimental results, and excellent agreement is achieved. Subsequent comparisons between the classical corrugated sandwich panels (without perforations) and corrugated sandwich panels with face plate perforations prove the face plate perforations are effective in improving the SAC and STL at low frequencies. Meanwhile, the acoustical resonance frequencies and bandwidths in SAC and STL curves are shown to decrease with increasing pore diameter and decreasing perforation ratio. Panels with either non-uniform perforated pore diameters or non-uniform perforation ratios can have better low-frequency SAC and STL than those with uniform pore diameters and perforation ratios. Results obtained in the present paper can help researchers to design superior multifunctional structures that aim at reducing both reflection and transmission with internal noise while maintaining high load-carrying capability. Further optimization work can be conducted based on corrugated sandwich panels with non-uniform perforations.

Acknowledgements

H. Meng was sponsored by China Scholarship Council as a joined Ph. D. student in Ecole Centrale de Lyon. This work was supported by the National Natural Science Foundation of China (51528501 and 11532009) and the Fundamental Research Funds for Central Universities (2014qngz12).

References

[1] Wang D-W, Ma L. Sound transmission through composite sandwich plate with pyramidal truss cores. Compos Struct 2017;164:104–17.
[2] Shengchun W, Zhaoxiang D, Weidong S. Sound transmission loss characteristics of unbounded orthotropic sandwich panels in bending vibration considering transverse shear deformation. Compos Struct 2010;92(12):2885–9.
[3] Song Y, Feng L, Wen J, Yu D, Wen X. Reduction of the sound transmission of a periodic sandwich plate using the stop band concept. Compos Struct 2015;128:428–36.
[4] Sadri M, Younesian D. Vibroacoustic analysis of a sandwich panel coupled with an enclosure cavity. Compos Struct 2016;146:159–75.
[5] Petrone G, D'Alessandro V, Franco F, De Rosa S. Numerical and experimental investigations on the acoustic power radiated by Aluminium Foam Sandwich panels. Compos Struct 2014;118:170–7.
[6] Liu Y, Daudin C. Analytical modelling of sound transmission through finite clamped double-wall sandwich panels lined with poroelastic materials. Compos Struct 2017;172:359–73.
[7] Liu Y, He C. Diffuse field sound transmission through sandwich composite cylindrical shells with poroelastic core and external mean flow. Compos Struct 2016;135:383–96.
[8] Shen C, Xin FX, Lu TJ. Sound transmission across composite laminate sandwiches: influence of orthogonal stiffeners and laminate layup. Compos Struct 2016;143:310–6.
[9] Wang T, Li S, Rajaram S, Nutt SR. Predicting the sound transmission loss of sandwich panels by statistical energy analysis approach. J Vib Acoust 2010;132(1). 011004:1–7.
[10] Xin FX, Lu TJ, Chen CQ. Sound transmission through simply supported finite double-panel partitions with enclosed air cavity. J Vib Acoust 2010;132(1). 011008: 1–11.
[11] Price AJ, Crocker MJ. Sound transmission through double panels using statistical energy analysis. J Acoust Soc Am 1970;47:683–93.
[12] Chazot JD, Guyader JL. Prediction of transmission loss of double panels with a patch-mobility method. J Acoust Soc Am 2007;121(1):267–78.
[13] Craik RJM. Non-resonant sound transmission through double walls using statistical energy analysis. Appl Acoust 2003;64(3):325–41.
[14] Xin FX, Lu TJ. Analytical and experimental investigation on transmission loss of clamped double panels: implication of boundary effects. J Acoust Soc Am 2009;125(3):1506–17.
[15] Sun W, Liu Y. Vibration analysis of hard-coated composite beam considering the strain dependent characteristic of coating material. Acta Mech Sinica 2016;32(4):731–42.
[16] Chazot JD, Guyader JL. Transmission loss of double panels filled with porogranular materials. J Acoust Soc Am 2009;126(6):3040–8.
[17] Doutres O, Atalla N. Acoustic contributions of a sound absorbing blanket placed in a double panel structure: absorption versus transmission. J Acoust Soc Am 2010;128(2):664–71.
[18] Bolton JS, Green E. Normal incidence sound transmission through double-panel systems lined with relatively stiff, partially reticulated polyurethane foam. Appl Acoust 1993;39:23–51.
[19] Panneton R, Atalla N. Numerical prediction of sound transmission through finite multilayer systems with poroelastic materials. J Acoust Soc Am 1996;100(1):346–54.
[20] Kang YJ, Bolton JS. A finite element model for sound transmission through foam-lined double-panel structures. J Acoust Soc Am 1996;99(5):2755–65.

[21] Bolton JS, Shiau NM, Kang YJ. Sound transmission through multi-panel structures lined with elastic porous materials. J Sound Vib 1996;191(3):317–47.
[22] Ghanbari M, Hossainpour S, Rezazadeh G. Studying thin film damping in a micro-beam resonator based on non-classical theories. Acta Mech Sinica 2016;32(3):369–79.
[23] Meng H, Xin FX, Lu TJ. External mean flow effects on sound transmission through acoustic absorptive sandwich structure. AIAA J 2012;50(10):2268–76.
[24] Wang TA, Sokolinsky VS, Rajaram S, Nutt SR. Assessment of sandwich models for the prediction of sound transmission loss in unidirectional sandwich panels. Appl Acoust 2005;66(3):245–62.
[25] Zhou R, Crocker MJ. Sound transmission loss of foam-filled honeycomb sandwich panels using statistical energy analysis and theoretical and measured dynamic properties. J Sound Vib 2010;329(6):673–86.
[26] Tang YY, Robinson JH, Silcox RJ. Sound transmission through a cylindrical sandwich shell with honeycomb core. 34th AIAA aerospace science meeting and exhibit 1996. pp. 877–886.
[27] Jung J-D, Hong S-Y, Song J-H, Kwon H-W. A study on transmission loss characteristics of honeycomb panel for offshore structures. J Appl Math Phys 2015;3:172.
[28] Griese D, Summers JD, Thompson L. The effect of honeycomb core geometry on the sound transmission performance of sandwich panels. J Vib Acoust 2015;137(2). 021011: 1–11.
[29] Rajaram S, Wang T, Nutt S. Sound transmission loss of honeycomb sandwich panels. Noise Cont Eng J 2006;54(2):106–15.
[30] Rajaram S, Nutt S. Measurement of sound transmission losses of honeycomb partitions with added gas layers. Noise Cont Eng J 2006;54(2):101–5.
[31] Shen C, Xin FX, Lu TJ. Theoretical model for sound transmission through finite sandwich structures with corrugated core. Int J Nonlinear Mech 2012;47(10):1066–72.
[32] Xin FX, Lu TJ. Effects of core topology on sound insulation performance of lightweight all-metallic sandwich panels. Mater Manuf Process 2011;26(9):1213–21.
[33] Bartolozzi G, Pierini M, Orrenius U, Baldanzini N. An equivalent material formulation for sinusoidal corrugated cores of structural sandwich panels. Compos Struct 2013;100:173–85.
[34] Maa D-Y. Theory and design of microperforated panel sound-absorbing constructions. Sci China 1975;18(1):38–50.
[35] Maa D-Y. Potential of microperforated panel absorber. J Acoust Soc Am 1998;104(5):2861–6.
[36] Atalla N, Sgard F. Modeling of perforated plates and screens using rigid frame porous models. J Sound Vib 2007;303(1):195–208.
[37] Rao KN, Munjal M. Experimental evaluation of impedance of perforates with grazing flow. J Sound Vib 1986;108(2):283–95.
[38] Lee DH, Kwon YP. Estimation of the absorption performance of multiple layer perforated panel systems by transfer matrix method. J Sound Vib 2004;278:847–60.
[39] Chen K-T. Study on the acoustic transmission loss of a rigid perforated screen. Appl Acoust 1996;47(4):303–18.
[40] Dupont T, Pavic G, Laulagnet B. Acoustic properties of lightweight micro-perforated plate systems. Acta Acust United Ac 2003;89(2):201–12.
[41] Toyoda M, Takahashi D. Sound transmission through a microperforated-panel structure with subdivided air cavities. J Acoust Soc Am 2008;124(6):3594–603.
[42] Bravo T, Maury C, Pinhède C. Sound absorption and transmission through flexible micro-perforated panels backed by an air layer and a thin plate. J Acoust Soc Am 2012;131(5):3853–63.
[43] Bravo T, Maury C, Pinhède C. Enhancing sound absorption and transmission through flexible multi-layer micro-perforated structures. J Acoust Soc Am 2013;134(5):3663–73.
[44] Mu RL, Toyoda M, Takahashi D. Sound insulation characteristics of multi-layer structures with a microperforated panel. Appl Acoust 2011;72(11):849–55.
[45] Conner BP, Manogharan GP, Martof AN, Rodomsky LM, Rodomsky CM, Jordan DC, et al. Making sense of 3-D printing: creating a map of additive manufacturing products and services. Addit Manuf 2014;1:64–76.
[46] Levy GN, Schindel R, Kruth J-P. Rapid manufacturing and rapid tooling with layer manufacturing (LM) technologies, state of the art and future perspectives. CIRP Annals-Manuf Technol 2003;52(2):589–609.
[47] Vaezi M, Seitz H, Yang S. A review on 3D micro-additive manufacturing technologies. Int J Adv Manuf Technol 2013;67(5–8):1721–54.
[48] Guo N, Leu MC. Additive manufacturing: technology, applications and research needs. Front Mech Eng 2013;8(3):215–43.
[49] Melchels FP, Domingos MA, Klein TJ, Malda J, Bartolo PJ, Hutmacher DW. Additive manufacturing of tissues and organs. Prog Polym Sci 2012;37(8):1079–104.
[50] Bolton JS, Yoo T, Olivieri O. Measurement of normal incidence transmission loss and other acoustical properties of materials placed in a standing wave tube. Brüel Kjær Tech Rev 2007;1:1–44.
[51] Maa D-Y. General theory and design of microperforated-panel absorbers. Acta Acust 1997;22(5):385–93.
[52] Zhang Z, Gu X. The theoretical and application study on a double layer microperforated sound absorption structure. J Sound Vib 1998;215(3):399–405.